SCIENTIFIC REPORTS

OPEN

Protecting the properties of monolayer MoS_2 on silicon based substrates with an atomically thin buffer

Received: 02 November 2015
Accepted: 13 January 2016
Published: 12 February 2016

Michael K. L. Man[1], Skylar Deckoff-Jones[1], Andrew Winchester[1], Guangsha Shi[2], Gautam Gupta[3], Aditya D. Mohite[3], Swastik Kar[4], Emmanouil Kioupakis[2], Saikat Talapatra[1,5] & Keshav M. Dani[1]

Semiconducting 2D materials, like transition metal dichalcogenides (TMDs), have gained much attention for their potential in opto-electronic devices, valleytronic schemes, and semi-conducting to metallic phase engineering. However, like graphene and other atomically thin materials, they lose key properties when placed on a substrate like silicon, including quenching of photoluminescence, distorted crystalline structure, and rough surface morphology. The ability to protect these properties of monolayer TMDs, such as molybdenum disulfide (MoS_2), on standard Si-based substrates, will enable their use in opto-electronic devices and scientific investigations. Here we show that an atomically thin buffer layer of hexagonal-boron nitride (hBN) protects the range of key opto-electronic, structural, and morphological properties of monolayer MoS_2 on Si-based substrates. The hBN buffer restores sharp diffraction patterns, improves monolayer flatness by nearly two-orders of magnitude, and causes over an order of magnitude enhancement in photoluminescence, compared to bare Si and SiO_2 substrates. Our demonstration provides a way of integrating MoS_2 and other 2D monolayers onto standard Si-substrates, thus furthering their technological applications and scientific investigations.

In recent years, transition metal dichalcogenides (TMDs) have gained much attention as semiconducting van der Waals materials that can be obtained in monolayer form[1–5]. Analogous to the technological importance of graphene for its electronic properties, the presence of a direct band gap in the visible part of the spectrum[2,3], as well as large optical absorption[6–9] and photoconductivity[10–12] in TMDs, particularly monolayer MoS_2, have cemented their importance in opto-electronic devices and applications, such as solar cell devices[9,13–15], photo-detectors[16–18], and other flexible opto-electronics[19]. Recent demonstrations have suggested the utility of MoS_2 in spin and valleytronic devices[20–22], as well as nanoelectronic devices with metallic and semiconducting phases[23–25]. However, like most atomically thin 2D materials, when placed on a substrate, interactions impact key opto-electronic, structural, and physical properties of monolayer MoS_2, preventing its full realization for potential technological applications. For example, quenching of photoluminescence on silicon[2,3] inhibits its utility in silicon-integrated valleytronic and spintronic devices. Similarly, diffuse electron diffraction patterns on Si and SiO_2[26] suggest a distorted crystalline structure or poor surface morphology, which impacts device performance[27]. Substrate interactions also inhibit the study of phase-engineered MoS_2 opto-electronic devices[23,24], where crystalline structure provides an important characterization tool for the different metallic and semiconducting phases. Thus the ability to integrate monolayer MoS_2 onto standard Si-devices, while simultaneously protecting a wide range of its key properties, is important for scientific and technological applications of MoS_2.

[1]Femtosecond Spectroscopy Unit, Okinawa Institute of Science and Technology Graduate University, Onna, Okinawa, 904-0495 Japan. [2]Department of Materials Science and Engineering, University of Michigan, 2106 H. H. Dow Bldg, 2300 Hayward St., Ann Arbor, MI 48109, USA. [3]Material Synthesis and Integrated Devices, MPA-11, Los Alamos National Laboratory, Los Alamos, NM 87545, USA. [4]Department of Physics, Northeastern University, Boston, Massachusetts 02115, USA. [5]Department of Physics, Southern Illinois University Carbondale, Carbondale, Illinois 62901, USA. Correspondence and requests for materials should be addressed to M.K.L.M. (email: michael.man@oist.jp)

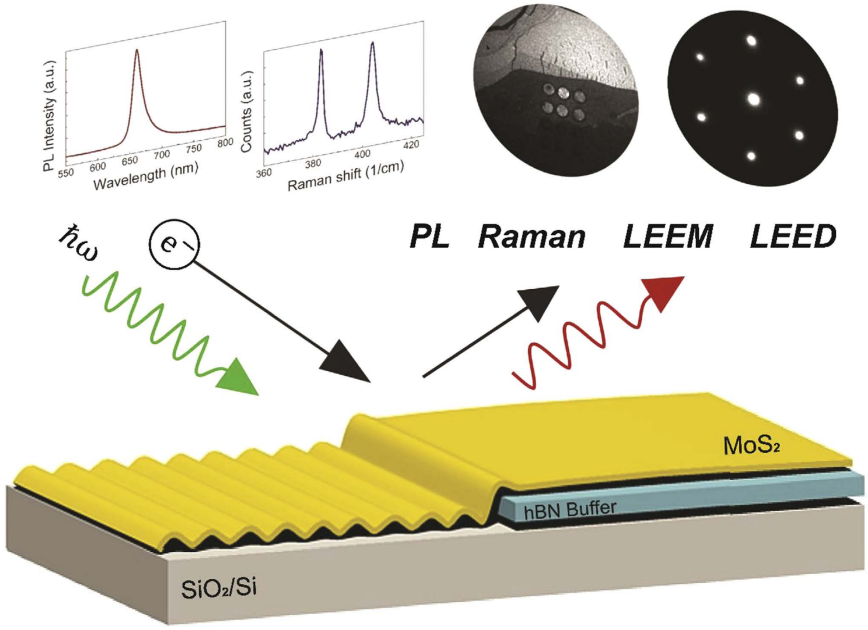

Figure 1. Schematic of the characterization of monolayer MoS_2 with an atomically thin hBN buffer on Si-based substrates. We characterize a range of key properties including photoluminescence (PL), Raman, Low Energy Electron Microscope (LEEM) images, Low Energy Electron Diffraction (LEED), and surface morphology of the monolayer with and without the buffer. On the bare substrate, we observe diffuse electron diffraction, quenched PL, quenched Raman, and a rough surface. The presence of the hBN buffer results in an order of magnitude stronger PL, Raman, sharper electron diffraction, and flat surface morphologies.

Given the practical requirements of substrates for 2D materials, a number of studies have explored substrate interactions for MoS_2 and other 2D crystals[2–4,26,28–31]. In MoS_2, electron probes of the surface structure noted the lack of a sharp diffraction pattern for monolayer samples on Si and SiO_2 for mechanically exfoliated, as well as in chemical vapor deposition (CVD) grown crystals[26]. Atomic force microscopy studies have shown a strong dependence of surface roughness on the underlying substrate[29]. Similarly, reports of photoluminescence quenching on Si[2,3] and SiO_2[4,28] were attributed to charge transfer from the substrate to monolayer MoS_2[4,28]. Other bulk substrates[4] such as hBN, $LaAlO_3$ and $SrTiO_3$ were shown to protect photoluminescence, by preventing such a charge transfer, but these lack easy-integration into standard electronics processing technologies. On the other hand, atomically thin sheets of hBN on Si-based substrates can easily be integrated into Si-based electronic devices and have been shown to improve electron mobilities[6,32,33]. However, the ability of an atomically thin buffer layer to protect optical properties by preventing charge transfer[34], or to restore sharp crystallinity by screening substrate interactions, remains unexplored. In general, a suitable solution to integrate monolayer MoS_2 into standard Si-based processing technologies, while protecting the wide range of opto-electronic, structural and morphological properties of MoS_2 remains elusive.

In this article, we demonstrate that an atomically thin buffer layer of hBN simultaneously protects the range of key opto-electronic, structural and morphological properties of monolayer MoS_2 on Si-based substrates (Fig. 1). Using microprobe-Low Energy Electron Diffraction (μ-LEED), we show that monolayer MoS_2 on bare Si and SiO_2 substrates exhibits a diffuse diffraction pattern and a warped surface morphology. On the other hand, the atomically thin hBN buffer layer restores sharp diffraction patterns and results in an extremely flat 2D morphology, with over an order of magnitude less surface roughness. Using micro-photoluminescence and micro-Raman, we further show that the photoluminescence and Raman with the hBN buffer is over two orders of magnitude larger than on bare Si, and is enhanced compared to even suspended samples. This ability to protect a wide range of key properties of monolayer MoS_2 on Si-based substrates thus enables sophisticated applications such as valleytronics[20–22] and phase-engineered devices[23–25], where the preservation of multiple intrinsic properties of MoS_2 are simultaneously required.

To study the effect of an atomically thin hBN buffer layer between monolayer MoS_2 and Si based substrates, we prepared a variety of mechanically exfoliated samples using a viscoelastic stamp[35]. First, mono- to few-layer samples of MoS_2 were directly exfoliated on bare Si and SiO_2. These were compared to monolayer flakes suspended on a grid of 2.5 μm holes on Si. Finally, atomically thin buffer layers of hBN with 1–5 nm thickness were first exfoliated onto SiO_2/Si, followed by exfoliation of larger MoS_2 flakes on top. These structures were annealed at 200 °C for a few hours in an ultrahigh vacuum chamber. Further details of sample preparation are presented in the Methods Section. Optical images of the different samples are shown in Fig. 2(a–d), with the regions of monolayer MoS_2 identified by the dotted white line.

To study the structural and surface morphological properties of the MoS_2 flakes, we used a Low Energy Electron Microscope (LEEM) capable of measuring spatially resolved electron diffraction patterns with

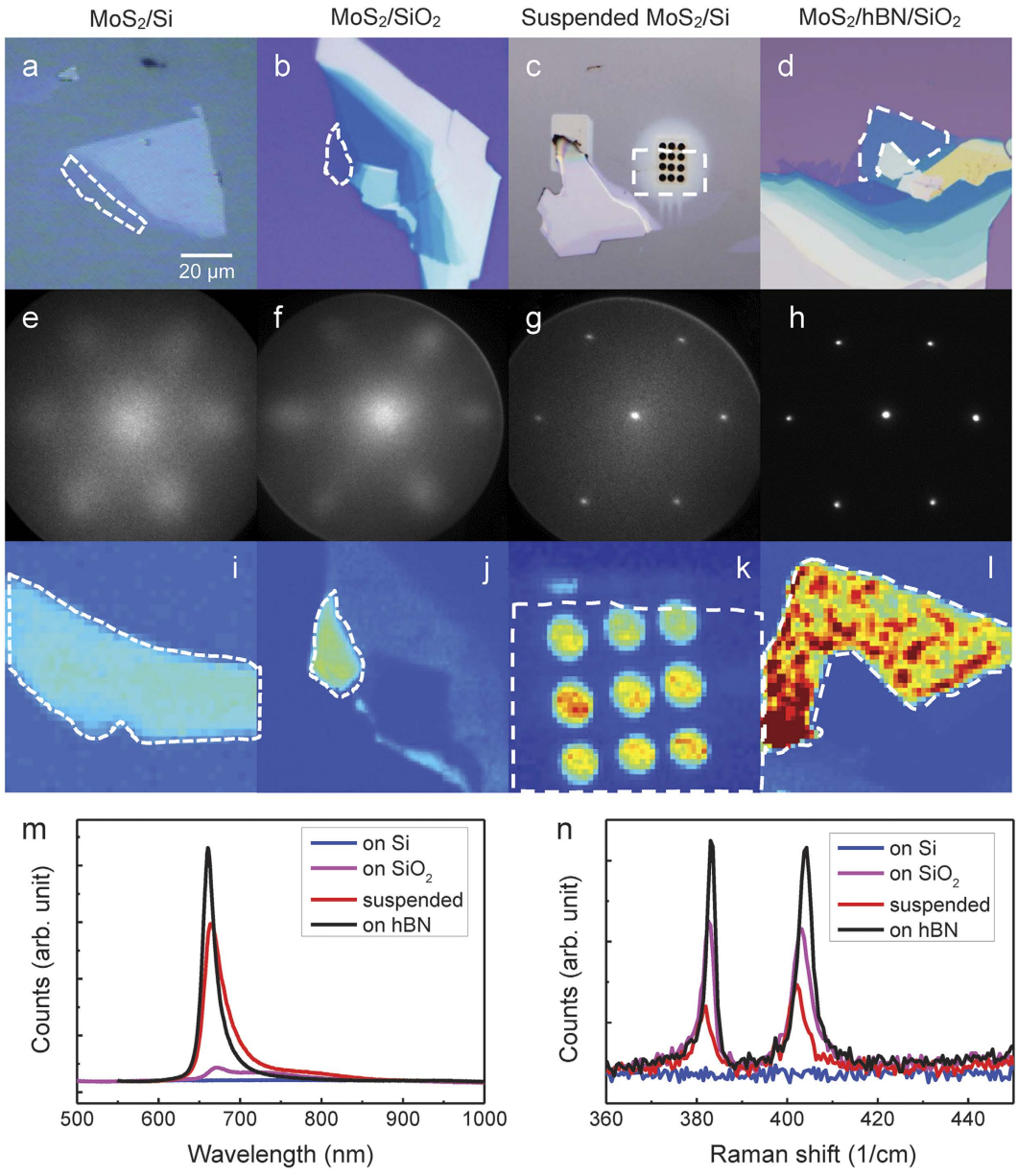

Figure 2. Optical, μ-LEED pattern, PL and Raman spectra of monolayer MoS_2 on different substrates. (**a–d**) shows optical images of the MoS_2 flakes, with monolayer areas outlined (white dashed line). In (**c**), the black circles are 2.5 μm diameter holes drilled into the Si substrate by focused ion beam with a suspended monolayer MoS_2 on top. (**e–h**) shows the μ-LEED pattern of monolayer MoS_2 using an electron beam of 250 nm diameter at 50 eV. Relatively weak and diffuse diffraction patterns are obtained for monolayer MoS_2 on top of Si and SiO_2, whereas for suspended MoS_2 and MoS_2 on top of hBN buffer, sharp, pristine diffraction patterns are observed. (**i–l**) are intensity maps of the PL peak with the color-scale optimized individually for visibility. Comparison of PL signal strength and Raman spectra of different samples are given in (**m**,**n**), respectively. The monolayer resting on the hBN buffer shows more than an order of magnitude increase in PL over the monolayer on bare Si or SiO_2.

sub-micron resolution. Opto-electronic properties were studied using commercial micro-PL and micro-Raman setups. Details of experimental conditions are presented in the Methods Section.

Electron diffraction obtained from monolayer MoS_2 placed on Si and SiO_2 substrates (Fig. 2e,f) shows a significantly weakened and diffuse diffraction pattern compared to suspended samples (Fig. 2g), indicating structural disorder or surface roughness. Similarly, PL maps (Fig. 2i–l) of the MoS_2 flakes on the different substrates allow us to distinguish the regions of monolayer, but show a significantly weakened PL on the Si and SiO_2 substrates compared to the suspended sample (Fig. 2m). We also observe a quenched Raman signal on Si (Fig. 2n). This weak electron diffraction, photoluminescence, and Raman on Si-based substrates limit the utility and integrability of MoS_2 in standard opto-electronic devices. In contrast, the presence of an atomically thin buffer layer of hBN protects the range of key structural and opto-electronic properties of MoS_2. As seen in Fig. 2(h,m,n), a protective

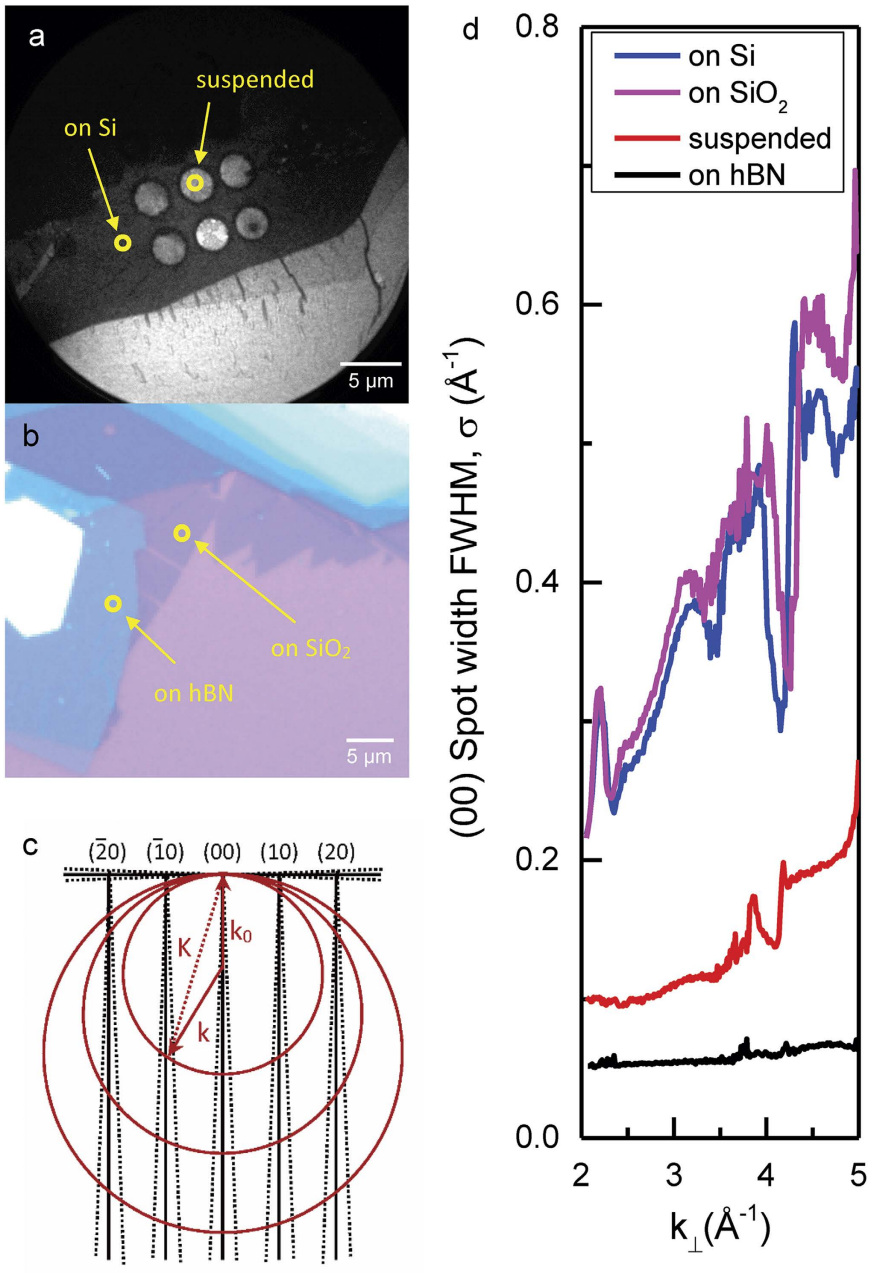

Figure 3. Comparing surface roughness of monolayer MoS_2 on different substrates. (**a**) LEEM images of MoS_2 flakes sitting on top of a holey Si substrate. (**b**) Optical image of an MoS_2 flake on SiO_2 with hBN buffer in between. Markers in (**a**,**b**) indicate positions where detailed LEED spot profile analyses were done. (**c**) explains the mechanism that causes broadening of the observed LEED diffraction pattern. A rough surface produces diffraction beams which spread out as a cones perpendicular to the sample surface, causing increased broadening with increasing incident electron energy. (**d**) The FWHM of the specular (00) diffraction beam–σ, with respect to the incident electron wave vector $k_\perp$. Superimposed on the resonant features due to few-layer effects, the overall linear increase in σ indicates a high degree of surface roughness of the MoS_2 on bare Si and SiO_2. A smaller slope in suspended MoS_2 shows a much reduced, but non-zero surface roughness in suspended samples, while the hBN buffer results in yet another order of magnitude decrease in surface roughness.

buffer layer of hBN recovers a sharp diffraction pattern, enhanced photoluminescence and Raman from monolayer MoS_2 by reducing substrate interactions.

To further explore the role of hBN in protecting these properties in MoS_2 and its potential applicability to other 2D monolayers, we study electron diffraction as a function of incident electron energy. The protective layer of hBN can be as thin as ~1 nm, as shown in Figs S1 and S2. In particular, we measure the broadening of the diffracted electron beam for different MoS_2 samples (Fig. 3). This allows us to distinguish between two important mechanisms that cause diffuse electron diffraction – a) lattice distortions or defects in the crystal structure, or b) surface roughness of the 2D crystal. In the case of lattice distortions, the broadening in the diffuse diffraction

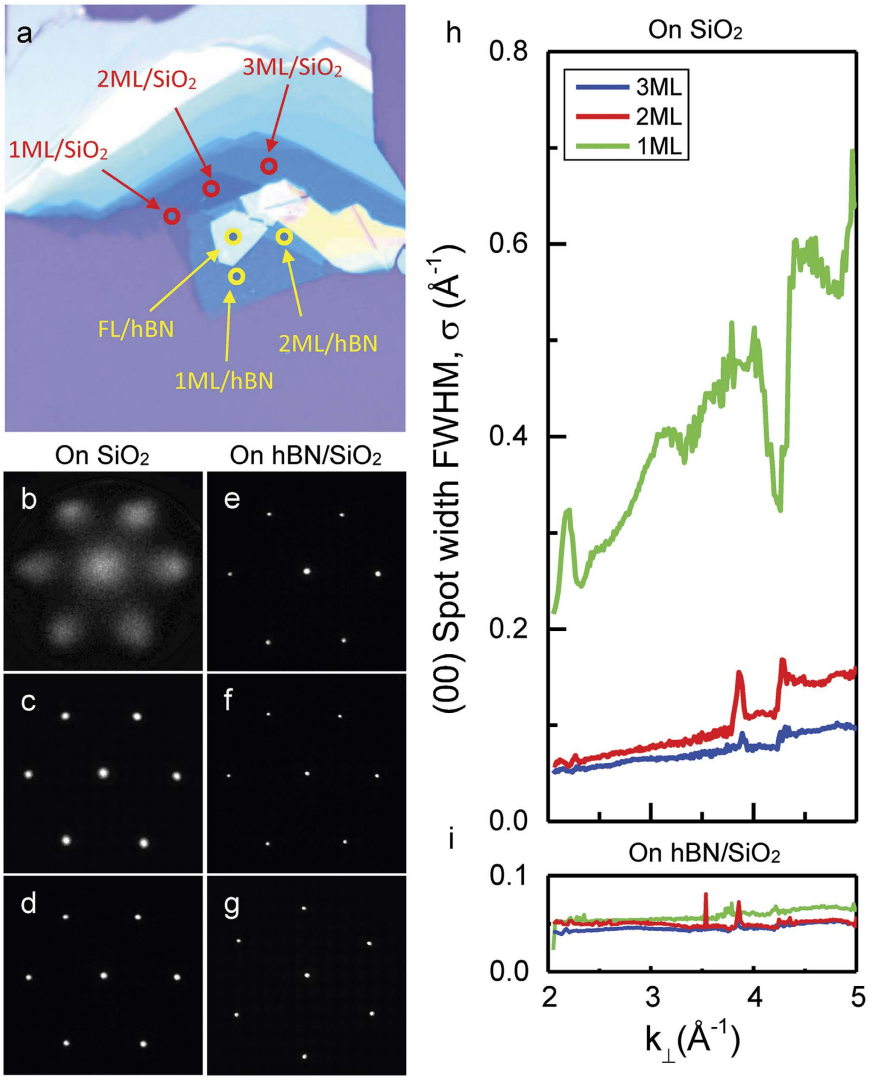

Figure 4. Surface roughness for mono-, bi- and few-layer MoS_2 on SiO_2 and on hBN buffer. (**a**) Optical image of a MoS_2 flake lying partially on top of SiO_2 and partially on top of a hBN buffer. (**b–d**) shows the μ-LEED pattern of 1 ML, 2 ML and 3 ML MoS_2 on SiO_2 and (**e–g**) shows the μ-LEED pattern of 1 ML, 2 ML and few layers MoS_2 on hBN. All LEED are taken at 50 eV. (**h**) The FWHM of the specular (00) diffraction beam–σ, versus incident electron wave vector $k_\perp$. The slope of the overall linear increase of σ versus $k_\perp$ shows the decreasing surface roughness from mono- to bi- to few-layer MoS_2 on SiO_2. On the other hand, MoS_2 on hBN displays negligible amount of beam broadening for all thickness.

pattern is independent of incident electron energy[36]. On the other hand, surface roughness leads to a linear increase in the FWHM of the diffuse diffraction pattern versus incident electron energy[37,38]. In this case, the roughness causes the scattered electron wave to propagate in directions deviating from the specular direction, with increasing deviations for increasing incident electron energy, as illustrated in Fig. 3(c).

By plotting the FWHM of the (00) diffraction beam (σ) versus incident electron wave vector $k_\perp$ for monolayer MoS_2 on different substrates (Fig. 3d), the mechanism for diffraction broadening can be elucidated. (Details of the fitting process are in the Methods Section). For the Si and SiO_2 substrates, we clearly see a linearly increasing σ superimposed on the resonant features resulting from structural effect in the samples. This indicates a high degree of roughness of the MoS_2 monolayer on top of Si and SiO_2. In comparison, one sees a much smaller σ, with a smaller linear increase in the suspended sample, indicating that the suspended sample exhibits much lower, but non-negligible surface roughness. In contrast, virtually no broadening of the diffraction pattern is detected for MoS_2 on hBN with almost no increase in σ as a function of the incident electron energy, indicating an extremely flat 2D monolayer.

Figure 4 compares the surface roughness for MoS_2 flakes of different thickness on both SiO_2 and hBN. Monolayer of MoS_2 shows the highest roughness on SiO_2 while films of greater thickness rapidly relax to form flat films. On the other hand, MoS_2 films of all thicknesses show fairly flat topologies on hBN. While our results typically explore samples of few-nm thick hBN, Fig. S1 shows that we obtain a sharp diffraction pattern and an extremely flat 2D monolayer even for a ~1 nm thick hBN buffer layer. Assuming that broadening of diffraction

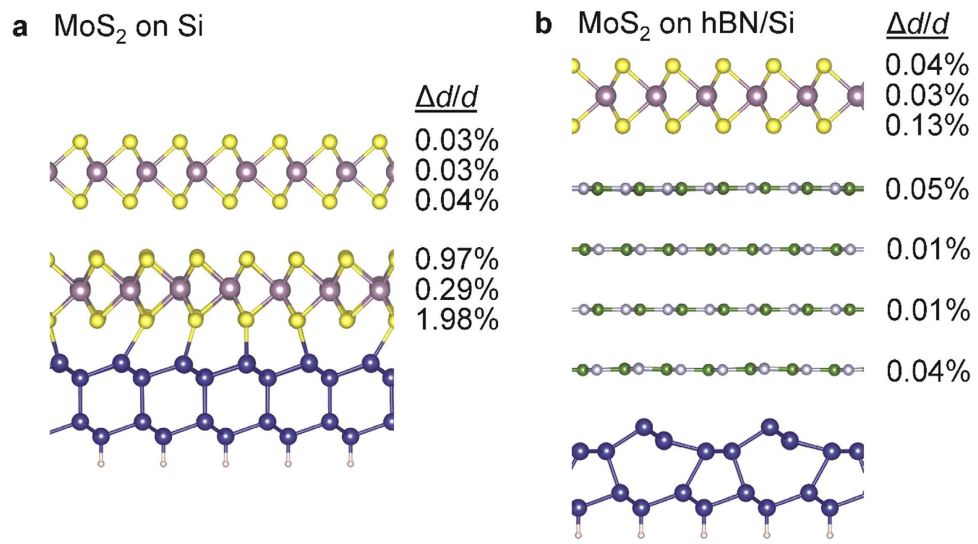

Figure 5. Density functional theory calculations of atomic interactions between MoS_2 and Si or hBN/Si surfaces. Relative variation of the in-plane lattice constant ($\Delta d/d$) for each atomic layer due to MoS_2-substrate interactions for (**a**) 2 ML MoS_2 on Si (111) and (**b**) 1 ML MoS_2 on 4 ML hBN on Si (111). (**a**) The bottom MoS_2 layer interacts strongly with dangling bonds on the Si surface and gets distorted, while the structure of the top MoS_2 layer is largely unaffected due to the weak van der Waals bond between the two layers. Si–S atoms with a distance shorter than 2.6 Å are connected with bonds for illustration. (**b**) Inserting 4 MLs of hBN between MoS_2 and the Si substrate significantly suppresses their interaction and distortion, as evident by the small fluctuation of in-plane bond lengths of MoS_2 and the 2×1 surface reconstruction of Si, due to weak van der Waals bonds between adjacent layers.

beams is caused by a Gaussian distribution of surface normal, surface roughness of the MoS_2 film can be quantified by the relation $\Delta\theta = \Delta k_{\parallel}/2\,k_{\perp}$, with a corresponding magnitude of 4.0°, 0.58°, and 0.48° for 1 ML, 2 ML, and 3 ML MoS_2 on SiO_2, respectively. We see a comparable value of 4.0° for 1 ML MoS_2 on bare Si. For suspended monolayer MoS_2, surface roughness can similarly be quantified as 0.7°, in agreement with previous experimental[39] and theoretical[27] results. In contrast, the roughness on hBN is given by 0.08°, reduced by more than an order of magnitude compared to SiO_2, Si or even the suspended samples. From our LEED measurements and analysis, we see that the surface roughness of monolayer MoS_2 on few-nm thick hBN is comparable to bulk MoS_2, which is consistent with previous AFM studies where the surface roughness of monolayer MoS_2 on bulk hBN was comparable to bulk MoS_2[29].

In order to further study the interaction of MoS_2 with Si and hBN/Si substrates, we performed density functional theory calculations (Fig. 5) to understand our experimental observations (See Methods section for details). For 2 ML MoS_2 directly deposited on Si (111), the bottom MoS_2 layer is significantly distorted with an in-plane S–S distance fluctuation of 1.98% (Fig. 5a). We attribute the distortion to bond formation between the bottom S and the surface Si atoms, as the shortest Si–S distance is 2.39 Å, which is comparable to the calculated Si–Si bond length (2.36 Å) and only 10% larger than the Si–S bond length in SiS_2 (2.13 Å)[40]. This implies that any Si surface roughness is transferred to the MoS_2 ML. The top MoS_2 layer of the 2 ML structure (and any subsequent layer farther away from the interface) is largely unaffected by interactions with the substrate because of weak van der Waals bonds between MoS_2 layers, which are much weaker than intralayer bonds. This result agrees with the experimental observation that the roughness of MoS_2 decreases for increasing numbers of MLs. In contrast, the MoS_2 ML distortions are one order of magnitude smaller (0.13% at most) if deposited on the 4 ML hBN/Si (111) surface (Fig. 5b). This is also attributed to the weak van der Waals bonds between layers and agrees with the flatness of MoS_2 on the hBN/Si surface observed in experiment. In addition, hBN interacts weakly with the substrate, as evident from the 2×1 reconstruction of the Si(111) surface[41], which shows that the Si surface atoms interact weakly with hBN. The smallest Si–N and Si–B distances are 3.21 Å and 3.28 Å, respectively, which are similar to the van der Waals bond length between hBN layers (3.35 Å)[42]. Moreover, the hBN layers are not distorted by the Si substrate. Therefore, as a result of the weak van der Waals interaction between all adjacent layers in the MoS_2/hBN/Si heterostructure, the hBN layers and the MoS_2 ML on top are weakly distorted, which agrees with the observed low roughness of both hBN and MoS_2 when deposited sequentially on Si (111).

In the triad of 2D materials – graphene as a metal, transition metal dichalcogenides as semiconductors, and hBN as an insulator, the role of hBN in protecting the electronic[32,33,43] and structural properties[33,43] of graphene has been previously reported. These properties also extend to the protection of other 2D monolayer properties, such as MoS_2, using bulk hBN, due to its inert chemical form, lack of dangling bonds, and flatness[44,45]. Our results show that hBN's protective capabilities can be achieved even with just a few atomic layers. We see that even with a few atomically thin layers of hBN on SiO_2/Si (Fig. S2), we obtain a stable, flat platform, which thereby prevents the overlying 2D monolayer from conforming to the roughness of the substrate.

Besides providing a stable, flat platform, atomically thin hBN needs to also screen interactions arising from the underlying Si-based substrate, which is not a consideration for bulk hBN substrates. DFT calculations for MoS_2 sitting directly atop Si, show a large distribution in the bond lengths in MoS_2, due to substrate interactions. Such distortions contribute to structural and morphological deformities observed via the diffuse crystalline patterns and quenched Raman signals, as well as modification of the electronic structure and optical responses[13,46]. In contrast, in the presence of an atomically thin layer of hBN, the bonds in MoS_2 are minimally distorted, with hBN acting as a barrier layer to minimize interactions with the Si substrate. Thus the ability of few-layer hBN to provide a flat platform and to minimize substrate interactions, provides insight into the observation of morphologically flat and undistorted crystals of monolayer MoS_2.

In addition to improvements in surface flatness and lattice distortion playing a role in protecting the opto-electronic properties[6,32,33], such as the PL enhancement seen here, we also expect that the few nm layer of hBN acts as a barrier to charge transfer from the SiO_2/Si substrate. This has been previously attributed as an important factor in PL quenching[4,47]. Lastly, we also note here the importance of annealing and cleaning the MoS_2/hBN heterostructure, which results in further improvements in the PL (Fig. S1), presumably due to removal of impurities and trapped states at the MoS_2/hBN interface[48]. Thus, overall we expect that the PL enhancement seen here is due to a combination of multiple factors – decreased surface roughness and lattice distortion due to reduced substrate interaction in the presence of the hBN buffer; the action of the hBN buffer as a barrier to charge transfer from the substrate; and decreased impurity/trapped states after annealing of the heterostructure sample.

In conclusion, we have shown that an atomically thin buffer layer of hBN simultaneously protects a range of key properties of monolayer MoS_2 on Si-based substrates. The atomically-thin hBN buffer allows for easy integration of monolayer MoS_2 into standard electronics devices, thus enhancing its utility in valleytronics, phase engineered nanoscale electronics, and other opto-electronic devices. Our results also have obvious implications for incorporating other 2D monolayers into standard Si-based devices, while protecting their opto-electronic, structural and morphological properties.

Methods

Sample preparation. MoS_2 flakes are prepared by exfoliation of MoS_2 single crystals supplied by Manchester Nanomaterials with the well-known scotch tape technique[49]. We transferred the MoS_2 flakes onto different substrates and created the MoS_2/hBN/SiO_2 heterostructure by an all-dry transfer method using a viscoelastic stamp (GelFilm from Gel-Pak) and a home-built micro-manipulator[35]. For MoS_2 on SiO_2, we used SiO_2/Si substrates with 300 nm of thermal oxide, which was first cleaned in an ultrasonic bath with acetone and then rinsed by methanol. For MoS_2 on Si, an oxide free Si surface is prepared by flash cleaning of the Si(111) wafer to a temperature close to the melting point of Si in the ultrahigh vacuum chamber (UHV) in LEEM. Sample cleanliness and oxide removal is confirmed by appearance of sharp (7×7) reconstructed surface with low energy electron diffraction[50]. For suspended MoS_2 flakes, hole of diameters of 2.5 μm and depth of 6 μm were drilled on the SiO_2/Si substrate by focused ion beam (FEI Helios NanoLab G3 UC). Before MoS_2 transfer, substrates with holes were first annealed in UHV chamber at 200 °C to remove Ga contamination from the ion milling process. For MoS_2/hBN/SiO_2 heterostructures, SiO_2/Si substrates were first cleaned by wet chemical method, as described above. hBN flakes of approximately few nm in thickness were prepared by exfoliation of an hBN single crystal (Manchester Nanomaterials) and then transferred onto the SiO_2/Si substrate using the GelFilm. Thin hBN flakes of uniform thickness were identified by AFM (Agilent 5500 AFM). MoS_2 flakes were transferred and positioned on top of the flat hBN flake using another GelFilm. The samples were then cleaned and annealed in an UHV chamber in preparation for μ-LEED and surface characterization measurements as described below. The cleaning and annealing process was also critical to observing the significant, order-of-magnitude enhancements in PL (Fig. S1b).

μ-LEED and Surface Roughness Characterization. Crystallinity and surface roughness of the MoS_2 flakes were investigated using a low energy electron microscope (LEEM) (Elmitec SPELEEM), which enables high resolution imaging of large sample areas (>100 μm) at resolution better than 10 nm, as well as microprobe-diffraction imaging. This allows access of structural information in sub-micron selected areas of less than 250 nm. LEEM uses very low energy electrons of few eV to image surfaces; hence it is extremely sensitive to surface contamination. Samples introduced in the LEEM imaging chamber are cleaned either by mild annealing at 200 °C for several hours or by illumination of electron beams which remove contamination from local area[38]. Samples cleaned by either method give similar diffraction patterns, revealing the crystallinity of the MoS_2 samples. We do not observe any degradation of crystallinity by performing any further annealing or electron illumination. Charging of the sample surface occurs during imaging, in particular, when the MoS_2 samples are on top of insulating substrates such as SiO_2. In our studies, we are able to eliminate detrimental charging effects by simultaneously illuminating the sample with an intense UV pulsed laser beam, which generates enough photoexcited carriers to neutralize any charging effects. Similarly, by using a very small incident electron beam of less than 250 nm in diameter during diffraction pattern imaging (μ-LEED), very little charging of the surface was observed. This could again be compensated by a very weak photon beam if needed.

Optical Characterization. Raman and photoluminescence characterization of the MoS_2 flakes were performed with a Nanofinder 30 (Tokyo instruments) with an excitation laser wavelength of 532 nm. Spatially resolved spot sizes of 0.5 μm were typically achieved in the measurement. PL spectra are taken at power of 1 mW and an exposure time of 10 s. Raman spectra are taken at a power of 2 mW, and an exposure time of 10 s with 5 accumulations.

First-Principles Calculations. Density Functional Theory calculations were performed using the Vienna Ab initio Simulation Package[51] with projector-augmented waves[52] and a cutoff of 350 eV. We used the

optB86b-vdW exchange-correlation functional[53] to account for the van der Waals interaction between the layered materials, which yields accurate lattice parameters for MoS_2[54]. Simulation supercells containing 230 (2 ML MoS_2 on Si) and 443 (1 ML MoS_2 on 4 ML hBN on Si) atoms were used to simulate the layer-substrate interactions. The positions of the Si atoms on the opposite side of the slab were fixed to the bulk values during atomic relaxation, and dangling bonds were passivated with H atoms. The structures are relaxed until the force on each atom is smaller than 8×10^{-3} eV/Å.

References

1. Li, H. *et al.* From Bulk to Monolayer MoS_2: Evolution of Raman Scattering. *Advanced Functional Materials* **22,** 1385–1390, doi: 10.1002/adfm.201102111 (2012).
2. Mak, K. F., Lee, C., Hone, J., Shan, J. & Heinz, T. F. Atomically thin MoS(2): a new direct-gap semiconductor. *Phys Rev Lett* **105,** 136805 (2010).
3. Scheuschner, N. *et al.* Photoluminescence of freestanding single- and few-layerMoS_2. *Physical Review B* **89,** 125406, doi: 10.1103/PhysRevB.89.125406 (2014).
4. Li, Y. *et al.* Photoluminescence of monolayer MoS_2 on $LaAlO_3$ and $SrTiO_3$ substrates. *Nanoscale* **6,** 15248–15254, doi: 10.1039/c4nr04602a (2014).
5. Yazyev, O. V. & Kis, A. MoS_2 and semiconductors in the flatland. *Materials Today* **18,** 20–30, doi: 10.1016/j.mattod.2014.07.005 (2015).
6. Lee, G. H. *et al.* Flexible and transparent MoS_2 field-effect transistors on hexagonal boron nitride-graphene heterostructures. *ACS Nano* **7,** 7931–7936, doi: 10.1021/nn402954e (2013).
7. Britnell, L. *et al.* Strong light-matter interactions in heterostructures of atomically thin films. *Science* **340,** 1311–1314, doi: 10.1126/science.1235547 (2013).
8. Tan, Y. *et al.* Polarization-dependent optical absorption of MoS(2) for refractive index sensing. *Sci Rep* **4,** 7523, doi: 10.1038/srep07523 (2014).
9. Bernardi, M., Palummo, M. & Grossman, J. C. Extraordinary sunlight absorption and one nanometer thick photovoltaics using two-dimensional monolayer materials. *Nano letters* **13,** 3664–3670, doi: 10.1021/nl401544y (2013).
10. Ghosh, S. *et al.* Ultrafast Intrinsic Photoresponse and Direct Evidence of Sub-gap States in Liquid Phase Exfoliated MoS_2 Thin Films. *Sci Rep* **5,** 11272, doi: 10.1038/srep11272 (2015).
11. Furchi, M. M., Polyushkin, D. K., Pospischil, A. & Mueller, T. Mechanisms of photoconductivity in atomically thin MoS_2. *Nano letters* **14,** 6165–6170, doi: 10.1021/nl502339q (2014).
12. Cunningham, G. *et al.* Photoconductivity of solution-processed MoS_2 films. *Journal of Materials Chemistry C* **1,** 6899–6904, doi: 10.1039/c3tc31402b (2013).
13. Feng, J., Qian, X., Huang, C.-W. & Li, J. Strain-engineered artificial atom as a broad-spectrum solar energy funnel. *Nature Photonics* **6,** 866–872, doi: 10.1038/nphoton.2012.285 (2012).
14. Tsai, M. L. *et al.* Monolayer MoS_2 heterojunction solar cells. *ACS Nano* **8,** 8317–8322, doi: 10.1021/nn502776h (2014).
15. Fontana, M. *et al.* Electron-hole transport and photovoltaic effect in gated MoS_2 Schottky junctions. *Sci Rep* **3,** 1634, doi: 10.1038/srep01634 (2013).
16. Zhang, W. *et al.* Ultrahigh-gain photodetectors based on atomically thin graphene-MoS_2 heterostructures. *Sci Rep* **4,** 3826, doi: 10.1038/srep03826 (2014).
17. Lopez-Sanchez, O., Lembke, D., Kayci, M., Radenovic, A. & Kis, A. Ultrasensitive photodetectors based on monolayer MoS_2. *Nat Nanotechnol* **8,** 497–501, doi: 10.1038/nnano.2013.100 (2013).
18. Yin, Z. *et al.* Single-layer MoS_2 phototransistors. *ACS Nano* **6,** 74–80, doi: 10.1021/nn2024557 (2012).
19. Wang, Q. H., Kalantar-Zadeh, K., Kis, A., Coleman, J. N. & Strano, M. S. Electronics and optoelectronics of two-dimensional transition metal dichalcogenides. *Nat Nanotechnol* **7,** 699–712, doi: 10.1038/nnano.2012.193 (2012).
20. Cao, T. *et al.* Valley-selective circular dichroism of monolayer molybdenum disulphide. *Nat Commun* **3,** 887, doi: 10.1038/ncomms1882 (2012).
21. Mai, C. *et al.* Many-body effects in valleytronics: direct measurement of valley lifetimes in single-layer MoS_2. *Nano letters* **14,** 202–206, doi: 10.1021/nl403742j (2014).
22. Zhu, Z. Y., Cheng, Y. C. & Schwingenschlogl, U. Giant spin-orbit-induced spin splitting in two-dimensional transition-metal dichalcogenide semiconductors. *Physical Review B* **84,** 153402, doi: 10.1103/PhysRevB.84.153402 (2011).
23. Kappera, R. *et al.* Phase-engineered low-resistance contacts for ultrathin MoS_2 transistors. *Nature materials* **13,** 1128–1134, doi: 10.1038/nmat4080 (2014).
24. Eda, G. *et al.* Coherent atomic and electronic heterostructures of single-layer MoS_2. *ACS Nano* **6,** 7311–7317, doi: 10.1021/nn302422x (2012).
25. Lin, Y. C., Dumcenco, D. O., Huang, Y. S. & Suenaga, K. Atomic mechanism of the semiconducting-to-metallic phase transition in single-layered MoS_2. *Nat Nanotechnol* **9,** 391–396, doi: 10.1038/nnano.2014.64 (2014).
26. Yeh, P.-C. *et al.* Probing substrate-dependent long-range surface structure of single-layer and multilayerMoS_2 by low-energy electron microscopy and microprobe diffraction. *Physical Review B* **89,** 155408, doi: 10.1103/PhysRevB.89.155408 (2014).
27. Miró, P., Ghorbani-Asl, M. & Heine, T. Spontaneous Ripple Formation in MoS_2 Monolayers: Electronic Structure and Transport Effects. *Advanced Materials* **25,** 5473–5475, doi: 10.1002/adma.201301492 (2013).
28. Buscema, M., Steele, G. A., van der Zant, H. S. J. & Castellanos-Gomez, A. The effect of the substrate on the Raman and photoluminescence emission of single-layer MoS_2. *Nano Research* **7,** 561–571, doi: 10.1007/s12274-014-0424-0 (2014).
29. Quereda, J., Castellanos-Gomez, A., Agrait, N. & Rubio-Bollinger, G. Single-layer MoS_2 roughness and sliding friction quenching by interaction with atomically flat substrates. *Applied Physics Letters* **105,** 053111, doi: 10.1063/1.4892650 (2014).
30. Liu, K.-K. *et al.* Growth of Large-Area and Highly Crystalline MoS_2 Thin Layers on Insulating Substrates. *Nano letters* **12,** 1538–1544, doi: 10.1021/nl2043612 (2012).
31. Ji, Q. *et al.* Epitaxial monolayer MoS_2 on mica with novel photoluminescence. *Nano letters* **13,** 3870–3877, doi: 10.1021/nl401938t (2013).
32. Cui, X. *et al.* Multi-terminal transport measurements of MoS_2 using a van der Waals heterostructure device platform. *Nat Nanotechnol* **10,** 534–540, doi: 10.1038/nnano.2015.70 (2015).
33. Dean, C. R. *et al.* Boron nitride substrates for high-quality graphene electronics. *Nat Nanotechnol* **5,** 722–726, doi: 10.1038/nnano.2010.172 (2010).
34. Li, L. H. *et al.* Dielectric screening in atomically thin boron nitride nanosheets. *Nano letters* **15,** 218–223, doi: 10.1021/nl503411a (2015).
35. Castellanos-Gomez, A. *et al.* Deterministic transfer of two-dimensional materials by all-dry viscoelastic stamping. *2D Materials* **1,** 011002, doi: 10.1088/2053-1583/1/1/011002 (2014).
36. Henzler, M. Measurement of surface defects by low-energy electron diffraction. *Applied Physics A Solids and Surfaces* **34,** 205–214, doi: 10.1007/bf00616574 (1984).

37. Knox, K. R. *et al.* Spectromicroscopy of single and multilayer graphene supported by a weakly interacting substrate. *Physical Review B* **78,** 201408, doi: 10.1103/PhysRevB.78.201408 (2008).
38. Locatelli, A. *et al.* Corrugation in exfoliated graphene: an electron microscopy and diffraction study. *ACS Nano* **4,** 4879–4889, doi: 10.1021/nn101116n (2010).
39. Brivio, J., Alexander, D. T. L. & Kis, A. Ripples and Layers in Ultrathin MoS_2 Membranes. *Nano letters* **11,** 5148–5153, doi: 10.1021/nl2022288 (2011).
40. Peters, J. & Krebs, B. Silicon disulphide and silicon diselenide: a reinvestigation. *Acta Crystallographica Section B Structural Crystallography and Crystal Chemistry* **38,** 1270–1272, doi: 10.1107/s0567740882005469 (1982).
41. Pandey, K. C. New π-Bonded Chain Model for Si(111)-(2×1) Surface. *Physical Review Letters* **47,** 1913–1917, doi: 10.1103/PhysRevLett.47.1913 (1981).
42. Brager, A. X-ray examination of the structure of boron nitride. *Acta Physicochim* URSS **7,** 699–706 (1937).
43. Decker, R. *et al.* Local electronic properties of graphene on a BN substrate via scanning tunneling microscopy. *Nano letters* **11,** 2291–2295, doi: 10.1021/nl2005115 (2011).
44. Kudin, K. N., Scuseria, G. E. & Yakobson, B. I. C2F,BN, and C nanoshell elasticity fromab initiocomputations. *Physical Review B* **64,** 235406, doi: 10.1103/PhysRevB.64.235406 (2001).
45. Song, L. *et al.* Large scale growth and characterization of atomic hexagonal boron nitride layers. *Nano letters* **10,** 3209–3215, doi: 10.1021/nl1022139 (2010).
46. Li, Y., Li, Y.-L., Araujo, C. M., Luo, W. & Ahuja, R. Single-layer MoS_2 as an efficient photocatalyst. *Catalysis Science & Technology* **3,** 2214, doi: 10.1039/c3cy00207a (2013).
47. Bhanu, U., Islam, M. R., Tetard, L. & Khondaker, S. I. Photoluminescence quenching in gold–MoS_2 hybrid nanoflakes. *Sci Rep* **4,** 5575, doi: 10.1038/srep05575 (2014).
48. Wang, F., Stepanov, P., Gray, M. & Lau, C. N. Annealing and transport studies of suspended molybdenum disulfide devices. *Nanotechnology* **26,** 105709, doi: 10.1088/0957-4484/26/10/105709 (2015).
49. Novoselov, K. S. *et al.* Electric field effect in atomically thin carbon films. *Science* **306,** 666–669, doi: 10.1126/science.1102896 (2004).
50. Telieps, W. & Bauer, E. The $(7 \times 7) \leftrightarrow (1 \times 1)$ phase transition on Si(111). *Surface Science* **162,** 163–168, doi: 10.1016/0039-6028(85)90890-8 (1985).
51. Kresse, G. & Furthmüller, J. Efficient iterative schemes forab initiototal-energy calculations using a plane-wave basis set. *Physical Review B* **54,** 11169–11186, doi: 10.1103/PhysRevB.54.11169 (1996).
52. Kresse, G. & Joubert, D. From ultrasoft pseudopotentials to the projector augmented-wave method. *Physical Review B* **59,** 1758–1775, doi: 10.1103/PhysRevB.59.1758 (1999).
53. Klimes, J., Bowler, D. R. & Michaelides, A. Chemical accuracy for the van der Waals density functional. *Journal of physics. Condensed matter : an Institute of Physics journal* **22,** 022201, doi: 10.1088/0953-8984/22/2/022201 (2010).
54. Peelaers, H. & Van de Walle, C. G. First-principles study of van der Waals interactions in MoS_2 and MoO_3. *Journal of physics. Condensed matter: an Institute of Physics journal* **26,** 305502, doi: 10.1088/0953-8984/26/30/305502 (2014).

Acknowledgements

GS and EK were supported by a National Science Foundation CAREER award through Grant No. DMR-1254314. Computational resources were provided by the National Energy Research Scientific Computing Center, supported by the Office of Science of the U.S. Department of Energy under Contract No. DE-AC02-05CH11231. ST acknowledges funding supported by the U.S. Army Research Office through a MURI grant# W911NF-11-1-0362. ST and KMD acknowledge funding support by Japan Society for the Promotion of Science (JSPS) through a fellowship (#L13521). SK gratefully acknowledges support from NSF ECCS 1351424. ADM and GG thank the LDRD program at LANL for funding for this work.

Author Contributions

M.K.L.M., S.D.J. and A.W. carried out all experiments and sample preparations. G.S. and E.K. designed, performed, and analyzed the density functional theory calculations. K.M.D. supervised all aspects of the project. G.G., A.M., S.K. and S.T. provided expertise and discussed about the results. All authors contributed in discussion and preparation of the manuscript.

Additional Information

Supplementary information accompanies this paper at http://www.nature.com/srep

Competing financial interests: The authors declare no competing financial interests.

How to cite this article: Man, M. K. L. *et al.* Protecting the properties of monolayer MoS_2 on silicon based substrates with an atomically thin buffer. *Sci. Rep.* **6**, 20890; doi: 10.1038/srep20890 (2016).